Energy levels and radiative data for Kr-like W^{38+} from MCDHF and RMBPT calculations

XueLing Guo[1,2,3]‡, Jon Grumer[1], Tomas Brage[1*], Ran Si[2,3], ChongYang Chen[2,3†], Per Jönsson[4], Kai Wang[5,6], Jun Yan[6,7], Roger Hutton[2,3], YaMing Zou[2,3]

[1] Division of Mathematical Physics, Department of Physics, Lund University, Sweden
[2] Shanghai EBIT Lab, Institute of Modern Physics, Department of Nuclear Science and Technology, Fudan University, Shanghai 200433, China
[3] Applied Ion Beam Physics Laboratory, Fudan University, Key Laboratory of the Ministry of Education, China
[4] Materials Science and Applied Mathematics, Malmö University, Sweden
[5] Hebei Key Lab of Optic-electronic Information and Materials, The College of Physics Science and Technology, Hebei University, Baoding 071002, China
[6] Institute of Applied Physics and Computational Mathematics, Beijing 100088, China
[7] Center for Applied Physics and Technology, Peking University, Beijing 100871, China

E-mail: * tomas.brage@fysik.lu.se

E-mail: † chychen@fudan.edu.cn

Abstract. Energies, transition rates, line strengths and lifetimes have been computed for all levels of the $4p^6$ and $4p^5 4d$ configurations of W^{38+} by using the multiconfiguration Dirac-Hartree-Fock method as well as relativistic many-body perturbation theory. We investigate systematically correlation, relativistic and QED effects on different properties, including excitation energies and transition rates. We demonstrate that it is important to include core-valence correlation of rather deep subshells (including $3d$ and $3p$) to reach close to spectroscopic accuracy for the transition energies. We also show that high multipole transitions (E3, M2) are important for the lifetime of some metastable levels of $4p^5 4d$ ($^3F_3$,$^1D_2$,$^3D_2$). The present results are in good agreement with experiments and of considerable higher accuracy than what has been reached in previous theoretical works.

PACS numbers: ...

Keywords: *atomic structure, energy levels, radiative data, lifetimes, electron correlation, tungsten*

‡ *Current address:* Department of Radiotherapy, Shanghai Changhai Hospital, Second Military Medical University, Shanghai 200433, China

1. Introduction

Tungsten is important in the diagnosis of astrophysical [1] and fusion plasmas [2, 3]. As an example of the latter, its physical properties makes it useful as a plasma-facing material in the International Tokamak Experimental Reactor (ITER) [4]. Accurate and reliable atomic data on tungsten ions are therefore in high demand, which has initiated a large number of both experimental and theoretical investigations (see e.g. the reviews in [5–8] and some examples of recent works in [9–20]).

The present work is focused on Krypton-like tungsten, W^{38+}, which has the ground and the first excited electron configurations $4s^24p^6$ and $4s^24p^54d$, outside a $1s^22s^22p^63s^23p^63d^{10}$ core. The ground configuration only have one $J = 0$ state while the first excited configuration has states with $0 \leq J \leq 4$. This will open up possibilities for many forbidden transitions - both inter-configurational to the ground state, and intra-configurational within the excited configuration (see figure 1).

Earlier theoretical models of W^{38+} [21–25] have been limited to just a few transitions and levels. On the experimental side, Radtke [21] observed two allowed E1 lines belonging to the transition array of $4p^54d - 4p^6$ ($J = 1 - J = 0$) for the first time at the Berlin electron-beam ion trap (EBIT), and later Utter [22] remeasured these lines and identified one more E1 line, and four other lines which were reported without classification. Around six years later, Radtke [23] measured three intra-configuration, forbidden M1 lines between $4p^54d$-levels.

On the theoretical side, Kramida *et al* [7] reported on energy levels and transition wavelengths obtained with the Cowan code [26] for the observed lines discussed above, which are collected in the NIST Atomic Spectra Database [27]. Fournier *et al* [24] performed calculations on W^{38+} by using the graphical angular momentum coupling code ANGLAR [28] and the fully relativistic parametric potential RELAC program by Klapisch *et al* [29]. They reported the transition properties for electric and magnetic dipole and quadrupole (E1, M1, E2, M2) in the X-ray and XUV region ($0 < \lambda < 20$ nm). However, they included only a limited treatment of correlation and ignored Quantum Electro-Dynamical (QED) corrections.

Recently Gaigalas *et al* [25] reported calculated energy levels and lifetimes of the $4p^6$ and $4p^54d$ configurations using the multi-configuration Dirac-Hartree-Fock method (MCDHF) of the GRASP2K program package [30] for Kr-like ions, including W^{38+}. Although there was good convergence in wavelengths as well as length and velocity values of the transition rate, their computed wavelengths for transitions from the $4p^54d$ excited states to the ground state are consistently shorter than the observed values. In addition, in their calculation, they assumed the Ni-like core as inactive and they computed lifetimes only from E1, E2, and M1 transitions between these levels.

Grumer *et al* [16] and Guo *et al* [31] emphasized the importance of deep-core-valence correlation effects in Ag-like ($4d^{10}4f$) and Co-like ($3p^63d^9$) ions. Karpuškienė *et al* [32] investigated the contribution of M2 and E3 transitions to the decay of metastable levels belonging to $4p^54d^{N+1}$ and $4p^64d^{N-1}4f$. It was shown that these high multipole

order transitions could significantly change the theoretical radiative lifetime values for some levels.

In this work we will therefore analyse the impact of core-valence correlation with deeper subshells on the transition energies and rates of Kr-like W^{38+}, as well as the effect of higher-order multipole transitions on the radiative lifetimes.

2. Theoretical Method

The aim of the present work is to accurately determine electric and magnetic dipole, quadrupole and octupole (E1, M1, E2, M2, E3) transition properties, involving all of the levels belonging to the ground and the first excited configuration $4s^24p^6$ and $4s^24p^54d$ of W^{38+}. Our first method of choice is the MCDHF method as implemented in the GRASP2K program suite [30]. In order to confirm the accuracy of the results, we have also performed an independent second-order relativistic many-body perturbation theory (RMBPT) calculation using the Flexible Atomic Code (FAC) [33].

Both of the methods start from the Dirac-Coulomb (DC) Hamiltonian

$$H_{\rm DC} = \sum_i \left[h_d(i) - V_{nuc}(r) \right] + \sum_{i<j} \left(\frac{1}{r_{ij}} \right) \tag{1}$$

where $h_d(i)$ is the Dirac Hamiltonian for one free electron, $V_{nuc}(r)$ is the nuclear potential Z/r_i corrected for a non-point nucleus, r_i is the radial coordinate of the electron i, and r_{ij} is the distance between the electrons i and j. Corrections to the instantaneous electron-electron interaction is introduced in both approaches through the frequency-independent Breit interaction [34, 35]

$$B_{ij} = -\frac{1}{2r_{ij}} \left[\alpha_{\mathbf{i}} \cdot \alpha_{\mathbf{j}} + \frac{(\alpha_{\mathbf{i}} \cdot \mathbf{r_{ij}})(\alpha_{\mathbf{j}} \cdot \mathbf{r_{ij}})}{r_{ij}^2} \right] \tag{2}$$

where α_i is the Pauli matrices. This results in the Dirac-Coulomb-Breit Hamiltonian

$$H_{\rm DCB} = H_{\rm DC} + \sum_{i<j} B_{ij} \quad . \tag{3}$$

It should be made clear that the Breit interaction in GRASP2K actually is evaluated from the full frequency-dependent expression of the transverse photon interaction (see equation 52 in [36]), but in this work it is evaluated in the long-wavelength limit of the exchanged photon which reduces to the frequency-independent expression above. Both approaches also allow for inclusion of self-energy (SE) and vacuum polarization (VP) [37, 38] QED corrections to first order. More details on how the Breit and QED contributions are implemented in the GRASP2K and FAC codes, will be given in the two following sections.

2.1. The GRASP2K multi-configuration Dirac-Hartree-Fock method

The MCDHF method is based on a representation of the atomic eigenstate - the atomic state function (ASF), $\Psi(\Gamma\pi J)$ - in terms of a linear combination of configuration state

functions (CSFs), $\Phi(\gamma_i \pi J)$,

$$\Psi(\Gamma \pi J) = \sum_i c_i \Phi(\gamma_i \pi J), \tag{4}$$

where π and J denote parity and total electronic angular momentum respectively, and the γ_i's are labels chosen to uniquely define the individual CSFs. The ASF label Γ is usually assigned according to the γ_i of the dominant CSF component. The CSFs are constructed from single-electron Dirac orbitals according to standard parity and angular momentum symmetry rules [39]. In the MCDHF approach, the coefficients c_i and the CSFs are determined by solving the coupled MCDHF integro-differential equations, based on the $H_{\rm DC}$ Hamiltonian and derived by using a variational approach [39], applying a self-consistent field (SCF) method. A restricted active space (RAS) [40] of CSFs is generated from an active set (AS) [41, 42] of orbitals together with choice of reference CSFs, the multireference (MR), and rules concerning active electrons and number of substitutions. An advantage of this approach is that the AS can be increased systematically, while monitoring the convergence of the atomic properties of interests, until an effectively complete basis set of CSFs has been found. The Breit interaction and dominant QED contributions (the self-energy and vacuum polarization) are then added in a final relativistic configuration interaction (RCI) calculation - i.e. without re-optimisation of the orbitals.

To be more specific, the Breit interaction is included as an additional interaction term in the total Hamiltonian (i.e. it is applied to all matrix elements) whereas the self-energy and vacuum polarization effects are included only as diagonal contributions (i.e. to first order). The most important radiative correction is the self-energy, which in GRASP2K is evaluated from tabulated one-electron (hydrogenic) values (see equation 55 and 56 in [36]) with reference values from [43]. The second most important radiative correction is vacuum polarization which is included as expectation values of the Uehling and Kjällén-Sabry potentials respectively [44] using the one-electron orbitals obtained in the MCDHF-SCF procedure (see equation 57 in [36]).

Once well-converged and effectively complete ASFs have been obtained, other physical properties, such as radiative transition rates, can be determined. The relativistic electric multipole transition operator is usually expressed in the length (Babushkin) or velocity (Coulomb) gauge [45], which should give equal results under the assumption that the ASFs are the exact eigensolutions. The level of agreement between these two gauges is therefore commonly used as a quality indicator of the computed approximate eigenstates - the ASFs.

The W^{38+} ground configuration $4p^6$ (even parity) and first excitation configuration $4p^5 4d$ (odd parity) are determined in independent calculations using the extended-optimal level (EOL) scheme with standard weights. A biorthogonal transformation technique is applied during the calculation of the E1, M2 and E3 transition parameters in order to deal with the non-orthogonality between the even and odd sets of orbitals [46].

2.1.1. Correlation Model: GRASP2K We define the electron core as $1s^2 2s^2 2p^6 3s^2 3p^6 3d^{10}$ and treat $4s, 4p$ and $4d$ as valence subshells. The AS is enlarged systematically according to

$$\begin{aligned}
\mathrm{AS}_1 &= \{4s, 4p, 4d, 4f\}\,, \\
\mathrm{AS}_2 &= \mathrm{AS}_1 + \{5s, 5p, 5d, 5f, 5g\}\,, \\
\mathrm{AS}_3 &= \mathrm{AS}_2 + \{6s, 6p, 6d, 6f, 6g, 6h\}\,, \\
\mathrm{AS}_4 &= \mathrm{AS}_3 + \{7s, 7p, 7d, 7f, 7g\}\,, \\
\mathrm{AS}_5 &= \mathrm{AS}_4 + \{7h, 7i\}\,.
\end{aligned}$$

We will present the results from three different approximations - a Dirac-Hartree-Fock (DHF) model where only one configuration is included for each parity, a valence-valence (VV) and finally a larger core-valence (CV) correlation model. Both the VV and the CV approaches are single-reference models (i.e. $4p^6$ and $4p^5 4d$ for the even and odd calculations respectively).

For the VV model, we include all single and double (SD) substitutions from the valence shells of the reference configuration. This approach is similar to the one used by Gaigalas *et al* [25], except that we included the $7h$ and $7i$ subshells in a final step.

Two CV models are employed in this work. In the initial one we include, in addition to the VV model, single substitution from the $3d$ core subshell which accounts for CV correlation with $3d$. We note that the impact from AS_5 in the VV model was small and choose to limit the active space at AS_4 (see the results section for details). The results from this first CV approach will be referred to as CV_{3d}.

In the second CV model we add CV correlation also with the $3p$-subshell, by allowing for single substitution from this subshell into the AS of orbitals. The results from these calculations will be referred to as CV_{3p}. It should be clarified that correlation with even deeper core-subshells ($3s$ and $2p$) were included in test calculations but found to have negligible effects on the properties we are interested in. The CV_{3p} model presents our largest and most accurate approach.

2.2. The FAC Relativistic Many-Body Perturbation Theory method

The theoretical basis of the RMBPT method, as implemented in the FAC code, is based on the Rayleigh-Schrödinger perturbation theory [47] and allows for a combination of configuration interaction and second-order many-body perturbation theory (Gu [33]). The approach is built on the H_{DCB}, which is split up into a zero-order, model Hamiltonian, H_0, and a perturbation, V, defined as,

$$H_0 = \sum_i [h_d(i) + U(r_i)], \tag{5}$$

$$V = -\sum_i \left[V_n(r) + U(r_i)\right] + \sum_{i<j} \left(\frac{1}{r_{ij}} + B_{ij}\right) \tag{6}$$

where the $U(r)$ represents a model potential including the screening effects of "other" electrons, chosen to make the perturbation as small as possible. $U(r_i)$ is approximated

by a local central potential and is derived from a Dirac-Fock-Slater self-consistent-field (SCF) calculation, which minimizes the weighted mean energy of the involved configurations.

A key feature of FAC is its ability to split up the solution space of the full Hamiltonian $H_{\rm DCB}$ into two subspaces - a model space, M, containing the most important reference configurations, and an orthogonal space, N, including the remaining ones. An all-order, configuration-interaction treatment of the full matrix is applied to the M-space. Contributions from the N-space is then included up to second order through the perturbation V. Several small corrections to the Hamiltonian are also included in the calculations, such as nuclear recoil, vacuum polarization, and electron self-energy. These are all taken into account with, to atomic structure theory, standard procedures, similar to as in e.g. GRASP2K [30]. More details on the theoretical method of FAC is discussed in refs. [17, 33, 48–51].

2.2.1. Correlation Model: FAC The present model space M is spanned by the states belonging to the lowest even configuration $4p^6$ and the first excited odd configuration $4p^5 4d$, while the N space contains the configurations formed by single and double excitations from the M space. For the single excitations, we included configurations with one electron with principal quantum number $n \leq 125$. For double excitations, configurations with one electron with $n \leq 65$ and a second with $n \leq 100$ are included. The maximum orbital quantum number was always set to $l_{max} = 15$. All three kinds of electron correlation (VV, CV, and CC) were in effect taken into account since we allow for excitations from all subshells. To investigate the convergence of our approach, we systematically monitor the results while increasing the N space step-by-step, as described in Fei *et al* [16]. From this we estimate the convergence to be within one part in a million.

3. Results and Discussions

3.1. Excitation energies

We present our final results for excitation energies of W^{38+} from the present MCDHF-CV_{3p} and RMBPT calculations in table 1, and compare them with other available theoretical results [24, 25] and the compilation data by the NIST Atomic Spectra Database [27]. The designation of the levels are given in LS-coupling, which is convenient but have an average purity of only 62%. For completeness, we also give the corresponding jj-coupling labels in table 1, which have an average purity of 98%, to be expected for a highly ionized system. Despite this we follow the convention to label the eigenstates in LS-coupling for the rest of this report.

An energy-level diagram including transition channels is shown in figure 1 where we indicate observed lines (solid arrow) as-well as lines that we predict should be observable due to having a predicted branching fraction larger than 20% (dashed, dotted and dash-

dotted).

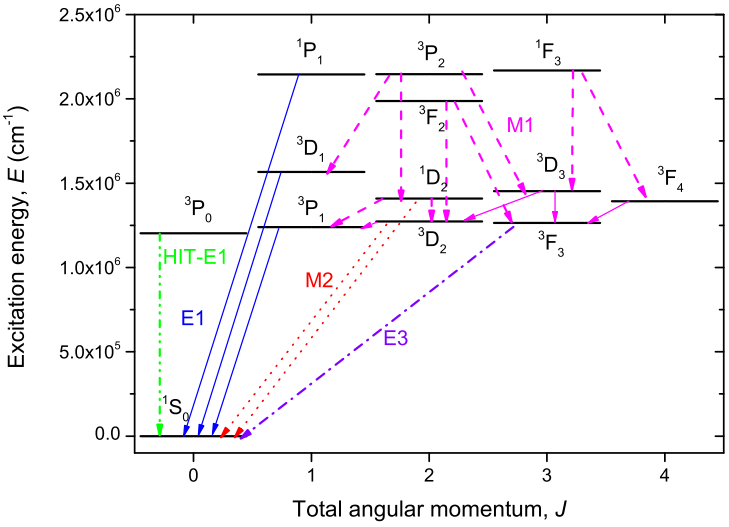

Figure 1. (Color online) Energy-level structure of the Kr-like W^{38+} showing the ground state $4p^6$ and the first excited configuration $4p^5 4d$. The 13 states are denoted by their dominate LS component. Solid arrows indicate observed lines (three E1 [21–23] and three M1 lines [23]). The dash, dot, and dash-dot arrow lines represent measurable M1, M2 or E3 transitions respectively, having a branching fraction of $B_F \geq 20\%$ (see table 3). The dash-dot-dot arrow line represents the hyperfine-induced-E1 (HIT-E1) transition which is not treated in this work.

The NIST [27] compiled energies in table 1 and in figure 2 originate from very different sources. Only three are truly experimental, namely the ones for $^3P_1$, $^3D_1$ and $^1P_1$ (represented by filled stars in the figure), which are derived from the measured wavelengths of corresponding E1 transitions [23]. The $^3P_0$ and $^1D_2$ (open stars) and $^3F_3$ (upper-half-filled star) energies are determined from semi-empirical Cowan code [26] calculations (Kramida *et al* [7]) and therefore put within brackets in the table. The remaining three ($^3D_2$, $^3D_3$ and $^3F_4$) levels are connected to the ground state via observed M1 lines (as seen from figure 1) to the $^3F_3$ level. Their predicted excitation energies are therefore derived from both a theoretical value for the lower $^3F_3$, as well as experimentally determined energies relative to this level. We illustrate this with the use of the $+x$ notation in the table and lower-half-filled stars in the figure.

It is clear that our CV_{3p} results reproduce well the experimental energies of the three $J = 1$ levels, within -0.15%, particularly for the $^3D_1$ and $^1P_1$. The present RMBPT method underestimates the energies of these two levels by about 0.2%, while the previous MCDHF [25] and RELAC-calculations [24] overestimate them by up to 0.5% and 1.2%, respectively. The discrepancies for these two levels is attributed to the slow correlation-convergence of their energies (see figure 3).

We note that the previous MCDHF work [25] included only VV correlation, and

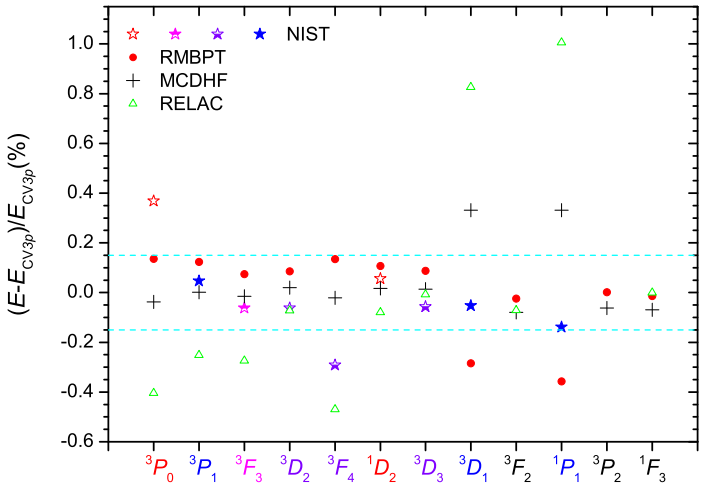

Figure 2. (Color online) Relative differences in excitation energies (in percent, %) from different theoretical and experimental works with the present MCDHF-CV_{3p}. The solid dots (•) represent our RMBPT results, while the crosses (+) and up-triangles (△) represent previous theoretical results, labelled MCDHF [25] and RELAC [24], respectively. The two dashed-lines represents a deviation of ±0.15%. The stars represent results from NIST-compilations, but note that only the solid stars indicates purely experimental results - see the text for details on this.

the RELAC calculation [24] only used a limited model for correlation effects and ignored the Breit and QED corrections. Since the excitation energies of two $J = 1$ level strongly depend on correlation effects, the RMBPT results could be improved by including higher order perturbation corrections, (as shown earlier for Be-like ions [52]).

The agreement between the NIST compiled energies and ours is also within 0.15%, with two exceptions - the $^3P_0$ and $^3F_4$ levels. The energy of the $^3P_0$ level is taken from Cowan code calculations [26] and differs from the CV_{3p} result by about -4430 cm^{-1}. The other large difference of 4057 cm^{-1} is for the semi-empirical energy of $^3F_4$. We note that there is a large deviation (2.5%) between the observed and calculated wavelength of $^3F_4 - ^3F_3$ transition, which puts the identification of this line into question.

In table 2 and figure 3 we illustrate the convergence of the excitation energies as a function of the size of the AS, of both the correlations models (VV and CV_{3p}). In the plots we define the relative change in energy when moving from AS_{n-1} to AS_n as

$$\delta E_{n,n-1} = E\left(\mathrm{AS}_n\right)/E\left(\mathrm{AS}_{n-1}\right) - 1 \quad . \tag{7}$$

It is clear that both models converge at the AS_4 step. The largest $\delta E_{4,3}$ value in the case of the CV_{3p} model is 0.05%. It is also interesting to note that two levels, the $^3D_1$ and $^1P_1$, converge considerably slower than the rest. The contributions from $7h$ and $7i$, investigated in the VV model, are very small ($\delta E_{5,4} < 0.01\%$) which supports that we

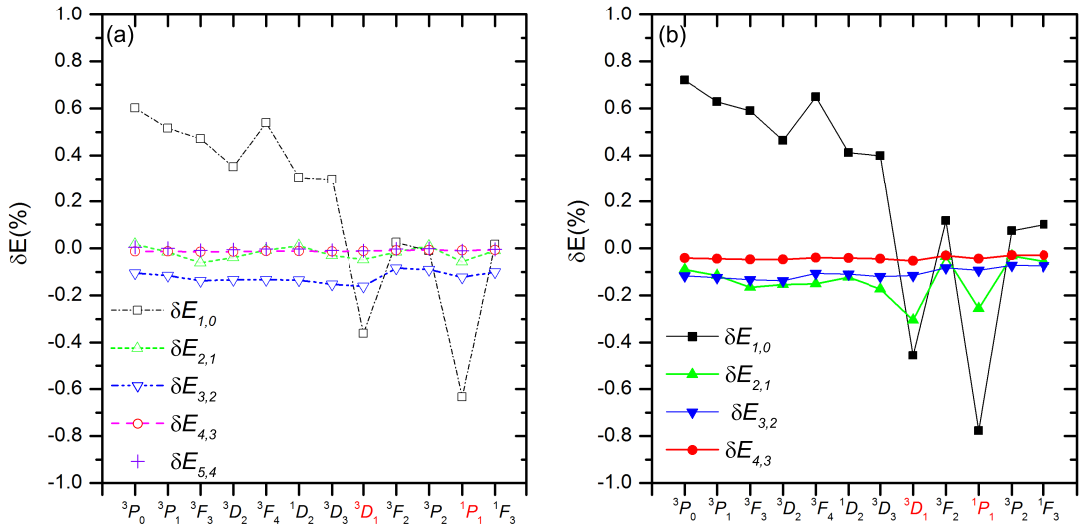

Figure 3. (Color online) Convergence of the calculated MCDHF energy levels as the active set of orbitals is enlarged. The relative energy quantity, $\delta E_{n,n-1}$, is defined in (7). The left panel gives results for the VV model, and the right for the CV_{3p} model (see the text for details).

have converged in the representation of high-l contributions, justifying the limitation of the CV model to AS_4.

In table 2 and figure 4 we show the contribution from correlation and Breit+QED (BQ) effects to the excitation energies. A relative contribution is defined by

$$\delta E_{model} = (E_{model} - E_{\mathrm{DHF}})/E_{\mathrm{DHF}} \tag{8}$$

which is illustrated in figure 4 for the MCDHF calculations. To compare, we also compute the corresponding property for the RMBPT method, where we use the RCI results for the M-space instead of DHF. It is clear that CV-contributions are important, especially for the $^3D_1$ and $^1P_1$ terms. What is more, we notice that when CV correlation with $3p$ is included, the order of the $^1P_1$ and $^3P_2$ levels is reversed. This explains the different order of these two terms in the previously performed MCDHF calculation [25].

The corrections from the Breit interaction and QED (SE + VP) effects, as listed in table 2, change little between the various calculation models. These contributions are also fairly constant within a jj-coupled term, defined as the pair of resulting j quantum numbers for the $4p^5$ and the $4d$ configurations, respectively, and given in table 1. The lowest four states belong to the $\left(\frac{3}{2},\frac{3}{2}\right)$ term and are all lowered about -4000 cm^{-1} by the Breit interaction and -1500 cm^{-1} by the self-energy. For the next term - $\left(\frac{3}{2},\frac{5}{2}\right)$ the corresponding numbers are about -7500 and -1200 cm^{-1}. Finally, the two highest terms - $\left(\frac{1}{2},\frac{5}{2}\right)$ and $\left(\frac{1}{2},\frac{3}{2}\right)$ are lowered by about -12000 and -15000 cm^{-1} by the Breit and -700 and -500 cm^{-1} by QED, respectively.

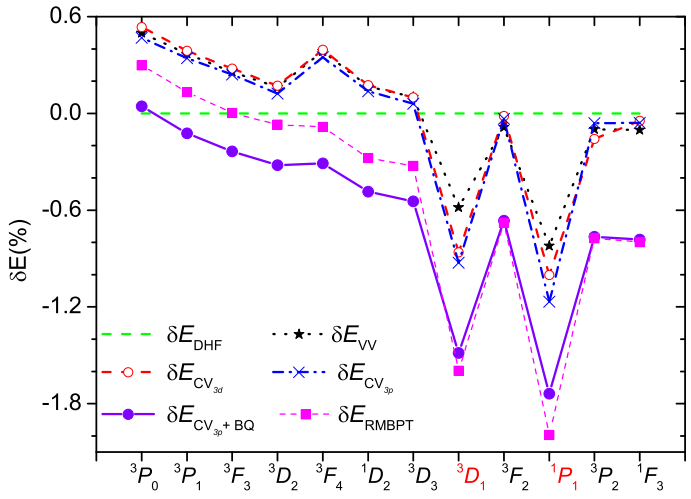

Figure 4. (Color online) Correlation and BQ (Breit+QED) contributions relative to the present DHF results, as defined in (8), for different models. For comparison we have also included the differences between the RMBPT and RCI results (excluding BQ effects). The relative contributions of the different models, eg. $\delta E_{\rm DHF}$, $\delta E_{\rm VV}$, $\delta E_{{\rm CV}_{3d}}$ and so on, are all in given in relation to $E_{\rm DHF}$. For example, $\delta E_{{\rm CV}_{3p}} = (E_{{\rm CV}_{3p}} - E_{\rm DHF})/E_{\rm DHF}$.

By considering the combined effect of correlation, both VV and CV, as well as Breit and QED, we find a small but significant discrepancy between our two methods - where RMBPT predicts larger excitation energies for lower levels, while for higher levels they are smaller. The difference is related to the different j-values of $4p^5$, that is the "fine structure splitting" between the 1/2 and 3/2 parents. Our RMBPT results seem to underestimate this separation, while the MCDHF model slightly overestimates it.

3.2. Wavelength and transition data

In table 3 we present properties for E1, M1, E2, M2 and E3 transitions between the included levels in our final MCDHF-CV_{3p} approach. For the electric multipoles, we only give the results using the length form of the transition operator, since it in general is considered to give more accurate results than the velocity form [25,53]. However, we do include an 'indicator of accuracy' factor, δS, for the line strength S [54],

$$\delta S = |S_l - S_v|/\max(S_l, S_v)$$

which represents the discrepancy in the length (S_l) and velocity (S_v) forms of the line strengths. In most cases δS are within 10%, except for some of the weaker transitions.

It is notable that the M2 transitions from $^3D_2$ and $^1D_2$ to the ground $^1S_0$ state account for more than 20% of their decays, and the E3 transition is the dominant decay channel from $^3F_3$. These high-multipole channels were not included in the earlier

MCDHF calculations [25], which explains why the resulting lifetimes for $^3D_2$, $^1D_2$ and $^3F_3$ differ from ours by about 22%, 30%, and 6 order of magnitudes, respectively (see table 1).

The lifetimes presented in table 1 show that the total correlation contribution generally is dominated by VV effects. The CV correlation does however still play a significant role for transitions involving the odd $J = 1$ states. For example, in the case of the E1 inter-configurational transition $^1P_1 - {}^1S_0$, the VV and CV correlation gives a contribution to the line strength of 17% and 7% while their contributions are 3% and 2% for the M1 intra-configurational transition of $^3P_2 - {}^3D_1$, respectively.

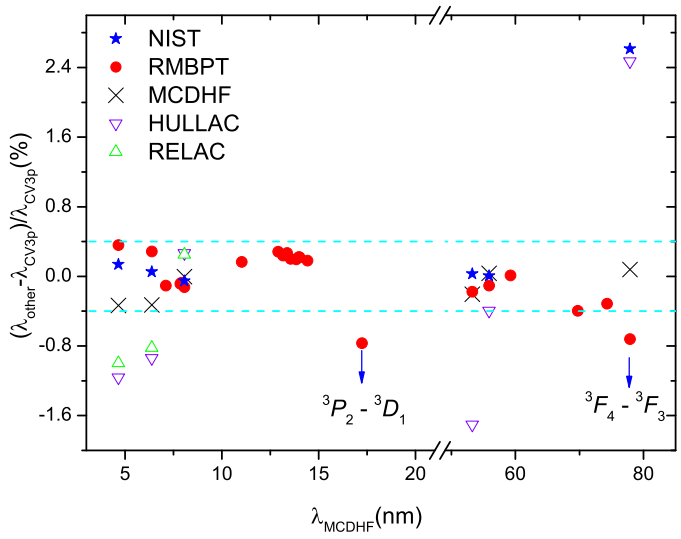

Figure 5. (Color online) Wavelength differences in percent (%) between the present CV_{3p} results and other the available theoretical work [23–25] as-well as experimental data collected by the NIST database [27]. The RMBPT label represents results from the present work, MCDHF from [25], HULLAC from [23] and RELAC from [24] (see text and table 4). The horizontal lines indicate differences of ±0.4%.

We present in table 4 and figure 5 a comparison of our theoretical wavelengths, from the present CV_{3p}, and other computed and measured ones for "observable" transitions (with branching fractions greater than 20%).

It is clear that our results agree with experiment for all cases except for the M1-transition $^3F_4 - {}^3F_3$. For this case the experimental wavelength disagrees with all theoretical ones, except for the HULLAC [23], which represents an approach with a much more limited treatment of correlation and other effects. Since the more elaborate calculations agree to within one percent in all cases, we recommend that the wavelength for $^3F_4 - {}^3F_3$ should be re-investigated.

3.2.1. Accuracy of MCDHF-CV$_{3p}$ transition properties In the following we investigate the accuracy of the transition properties represented by the lifetime (τ_j, $\tau_j = \frac{1}{\Sigma_i A^r_{ji}}$) of the included states. In the present work, all possible E1, E2, M1, M2, E3, M3 radiative decay channels are included, and their contributions are determined by the branching fractions B_F as listed in table 3.

The convergence trend of the lifetimes as a function of an increasing AS is shown in figure 6. It is clear that, as the basis set is increased systematically according to the description of the CV$_{3p}$ correlation model, the lifetimes converge to within 0.5% for almost all levels with the exception of $^3D_2$ which changes by around 0.7% in the last step.

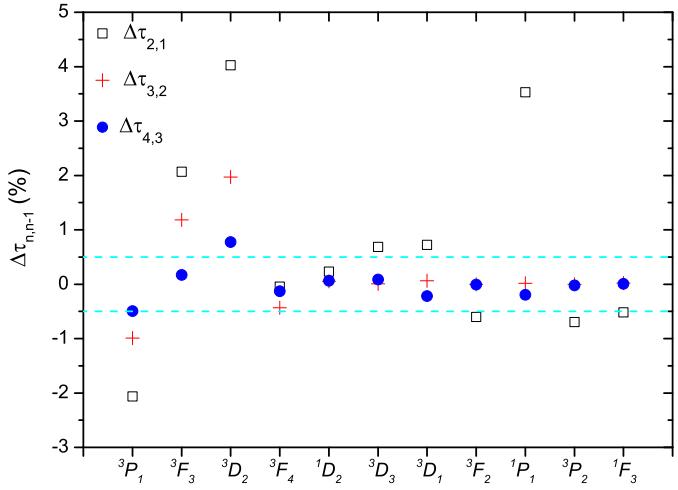

Figure 6. (Color online) Convergence of the computed lifetimes for the $4p^5 4d$-states using the MCDHF-CV$_{3p}$ model, where $\Delta\tau_{n,n-1} = [\tau(\mathrm{AS}_n) - \tau(\mathrm{AS}_{n-1})]/\tau(\mathrm{AS}_{n-1})$ is the relative change of the lifetime in percentage as the basis set is increased by one step. The horizontal lines indicate a relative differences of $\pm 0.5\%$.

4. Conclusions

In this paper we have presented transition properties for the energy levels of the $4p^6$ and $4p^5 4d$ configurations of Kr-like W^{38+}, including E1, E2, M1, M2 and E3 decay channels. Both MCDHF and RMBPT methods were used. The impact of correlation and relativistic effects on the excitation energies and other transition data have been investigated systematically. It was found that the core-valence correlation with the deep subshells $3d$ and $3p$ were of importance, especially for the higher $J = 1$ states, $^3D_1$, $^1P_1$, to reach good agreement with experiments. We have found excellent agreement between the present MCDHF-CV$_{3p}$ results and measured wavelengths collected in the NIST

database, except for the $^3F_4 - ^3F_3$ transition. We believe that the identification of this transition therefore is incorrect. We show that it is important to include higher multipole transitions since they might change the theoretical radiative lifetime values substantially for some levels. We found that the dominant decay channel of the metastable $^3F_3$ level is the E3 transition to the ground state, $^1S_0$. We also show that the M2 transitions from the $^3D_2$ and $^1D_2$ to $^1S_0$ contributes with about 20% to the their lifetimes.

Acknowledgements

This work was supported by the Swedish Research Council 2015-04842, the International Exchange Program Fund of doctoral students under the Fudan University Graduate School, the NSAF of China 11076009, National Natural Science Foundation of China 11374062, and the Chinese Association of Atomic and Molecular Data. It is also partially supported by the Chinese National Fusion Project for ITER 2015GB117000, and the Shanghai Leading Academic Discipline Project B107. Finally, the author X. L. Guo would especially like to thank the Nordic Centre at Fudan University for supporting an exchange between Lund and Fudan University.

References

[1] H. Hensberge and J. V. Santvoort *et al* . *Astron. Astrophys.*, 158:113, 1986.

[2] E. J. Doyle, W. A. Houlberg, Y. Kamada, V. Mukhovatov, T. H. Osborne, A. Polevoi, G. Bateman, J. W. Connor, J. G. Cordey, ITPA Transport Physics Topical Group, ITPA Confinement Database, Modelling Topical Group, ITPA Pedestal, and Edge Topical Group *et al* . *Nucl. Fusion*, 47:S18, 2007.

[3] J. Clementson and P. Beiersdorfer *et al* . *J. Phys. B: At. Mol. Opt. Phys*, 43:144009, 2010.

[4] A. J. H. Donne and A. E. Costley *et al* . *Nucl.Fusion*, 47:S337, 2007.

[5] A. E. Kramida and J. Reader. *At. Data Nucl. Data Tables*, 92:457 – 479, 2006.

[6] A. E. Kramida and T. Shirai. *J. Phys. Chem. Ref. Data*, 35:423, 2006.

[7] T. Shirai A. E. Kramida. *At. Data Nucl. Data Tables*, 95:305, 2009.

[8] A. Kramida. *Can. J. Phys.*, 89:551, 2011.

[9] U. I. Safronova and A. S. Safronova. *J. Phys. B: At. Mol. Opt. Phys*, 43:074026, 2010.

[10] P. Quinet. *J. Phys. B: At. Mol. Opt. Phys*, 45:025003, 2012.

[11] Z. Fei and R. Zhao *et al* . *Phys. Rev. A*, 86:062501, 2012.

[12] X. B. Ding and F. Koike *et al* . *J. Phys. B: At. Mol. Opt. Phys*, 45:035003, 2012.

[13] S. Aggarwal, A.K.S. Jha, and M. Man. *Can. J. Phys.*, 91:394–400, 2013.

[14] J. Grumer, R. Zhao, T. Brage, W. Li, S. Huldt, R. Hutton, and Y. Zou. *Phys. Rev. A*, 89:062511, 2014.

[15] J. Clementson and P. Beiersdorfer *et al* . *At. Data Nucl. Data Tables*, 100:577–649, 2014.

[16] Z. Fei, W Li, and J *et al* Grumer. *Phys. Rev. A*, 90:052517, 2014.

[17] X. L. Guo, M. Huang, J. Yan, S. Li, R. Si, C. Y. Li, C. Y. Chen, Y. S. Wang, and Y. M. Zou. *J. Phys. B: At. Mol. Opt. Phys*, 48:144020, 2015.

[18] M. L. Qiu, W. X. Li, Z. Z. Zhao, Y. Yang, J. Xiao, T. Brage, R. Hutton, and Y. Zou. *J. Phys. B: At., Mol. Opt. Phys.*, 48(14):144029, 2015.

[19] M L Qiu, R F Zhao, X L Guo, Z Z Zhao, W X Li, S Y Du, J Xiao, K Yao, C Y Chen, R Hutton, and Y Zou. Investigation of transitions between metastable levels of the first excited configuration of palladium-like tungsten. *J. Phys. B: At., Mol. Opt. Phys.*, 47:175002, 2014.

[20] Z. Z. Zhao, M. L. Qiu, R. F. Zhao, W. X. Li, X. L. Guo, J. Xiao, C. Y. Chen, Y. M. Zou, and R. Hutton. *J. Phys. B: At., Mol. Opt. Phys.*, 48:115004, 2015.

[21] R. Radtke and Biedermann *et al* . *Phys. Rev. A*, 64:012720, 2001.

[22] S. B. Utter, P. Beiersdorfer, and E. Trábert. *Can. J. Phys.*, 80:1503–1515, 2002.

[23] R Radtke, C Biedermann, G Fussmann, JL Schwob, P Mandelbaum, and R Doron. Measured line spectra and calculated atomic physics data for highly charged tungsten ions. *Atomic and Plasma-Material Interaction Data for Fusion; Clark, RE, Ed*, 13:45–66, 2007.

[24] K. B. Fournier. *At. Data Nucl. Data Tables*, 68:1 – 48, 1998.

[25] G. Gaigalas, P. Rynkun, and C. F. Fischer. *Phys. Rev. A*, 91:022509, 2015.

[26] R. D. Cowan. University of California Press, Berkeley, 1981.

[27] A. Kramida, Yu. Ralchenko, J. Reader, and NIST ASD Team. *http://physics.nist.gov/asd*, 2014.

[28] A. Bar-Shalom and M. Klapisch. *Comput. Phys. Commun*, 50:375 – 393, 1988.

[29] M. Klapisch. *Comput. Phys. Commun*, 2:239 – 260, 1971.

[30] P. Jönsson and G. Gaigalas *et al* . *Comput. Phys. Commun*, 184:2197 – 2203, 2013.

[31] X. L. Guo *et al* . *Phys. Rev. A (submitted)*.

[32] R. Karpuškienė, P. Bogdanovich, and R. Kisielius. *Phys. Rev. A*, 88:022519, 2013.

[33] M. F. Gu and T. Holczer *et al* . *The Astro.Phys.J*, 641:1227, 2006.

[34] I. P. Grant and N. C. Pyper. *J. Phys. B: At. Mol. Phys*, 9:761, 1976.

[35] F. A. Parpia, C. F. Fischer, and I. P. Grant. *Comput. Phys. Commun.*, 94:249 – 271, 1996.

[36] K.G. Dyall, I.P. Grant, C.T. Johnson, F.A. Parpia, and E.P. Plummer. Grasp: A general-purpose relativistic atomic structure program. *Computer Physics Communications*, 55(3):425–456, 1989.

[37] P. J. Mohr. *Phys. Rev. A*, 26:2338–2354, 1982.

[38] B.J. McKenzie, I.P. Grant, and P.H. Norrington. *Comput. Phys. Commun*, 21:233 – 246, 1980.
[39] I. P. Grant and B.J. McKenzie *et al* . *Comput. Phys. Commun*, 21:207 – 231, 1980.
[40] T. Brage and C. F. Fischer. *Phys .Scr*, 47:18 – 28, 1993.
[41] B. O. Roos, P. R. Taylor, and P. E.M. Sigbahn. *Che.Phys*, 48:157 – 173, 1980.
[42] J. Olsen and Björn O Roos *et al* . *The Journal of Chemical Physics*, 89:2185–2192, 1988.
[43] Peter J. Mohr. Energy levels of hydrogen-like atoms predicted by quantum electrodynamics. *Atomic Data and Nuclear Data Tables*, 29(3):453 – 466, 1983.
[44] L. Wayne Fullerton and G. A. Rinker. Accurate and efficient methods for the evaluation of vacuum-polarization potentials of order $z\alpha$ and $z\alpha^2$. *Phys. Rev. A*, 13:1283–1287, Mar 1976.
[45] I. P. Grant. *J. Phys. B: At. Mol. Phys*, 7:1458, 1974.
[46] J. Olsen and M. R Godefroid *et al* . *Phys. Rev. E*, 52:4499–4508, 1995.
[47] I. Lindgren. *J. Phys. B: At. Mol. Opt. Phys*, 7:2441, 1974.
[48] M. F. Gu. *Astrophys. J. Suppl. Ser.*, 169:154–158, 2007.
[49] R. Si, X. L. Guo, J. Yan, C. Y. Li, S. Li, M. Huang, C. Y. Chen, Y. S. Wang, and Y. M. Zou. *Journal of Quantitative Spectroscopy and Radiative Transfer*, 163:7 – 23, 2015.
[50] K. Wang, D. F. Li, H. T. Liu, X. Y. Han, B. Duan, C. Y. Li, J. G. Li, X. L. Guo, C. Y. Chen, and J. Yan. *The Astrophys. J. Suppl. Ser.*, 215:26, 2014.
[51] K. Wang, X. L. Guo, H. T. Liu, D. F. Li, F. Y. Long, X. Y. Han, B. Duan, J. G. Li, M. Huang, Y. S. Wang, R. Hutton, Y. M. Zou, J. L. Zeng, C. Y. Chen, and J. Yan. *The Astrophys. J. Suppl. Ser.*, 218(2):16, 2015.
[52] H. C. Ho, W. R. Johnson, S. A. Blundell, and M. S. Safronova. *Phys. Rev. A*, 74:022510, 2006.
[53] C. F. Fischer. *J. Phys. B: At. Mol. Opt. Phys*, 43:074020, 2010.
[54] C. F. Fischer. *Phys. Scr.*, 2009:014019, 2009.

Table 1: Excitation energies (E, in cm^{-1}) relative to the ground state and lifetimes (τ, in s) for levels of the $4p^6$ and $4p^5 4d$ configuration of W^{38+} from the present calculation and previous data. *a* - [27]; *b* - present work; *c* - [25]; *d* - [24].

LS	jj	$E^a_{\rm NIST}$	$E^b_{{\rm CV}_{3p}}$	$E^b_{\rm RMBPT}$	$E^c_{\rm MCDHF}$	$E^d_{\rm RELAC}$	$\tau^b_{\rm DHF}$	$\tau^b_{\rm VV}$	$\tau^b_{{\rm CV}_{3p}}$	$\tau^c_{\rm MCDHF}$
$^1S^e_0$	$(0,0)_0$	0	0	0	0	0	– – –	– – –	– – –	– – –
$^3P^o_0$	$(\frac{3}{2},\frac{3}{2})_0$	[1208000]	1203570	1205201	1203118	1198704	– – –	– – –	– – –	– – –
$^3P^o_1$	$(\frac{3}{2},\frac{3}{2})_1$	1240000	1239427	1240953	1239448	1236314	4.005[−10]	3.832[−10]	3.797[−10]	3.82[−10]
$^3F^o_3$	$(\frac{3}{2},\frac{3}{2})_3$	$[1264000]+x$	1264782	1265721	1264594	1261312	4.849[−02]	4.685[−02]	4.743[−02]	4.82[+04]
$^3D^o_2$	$(\frac{3}{2},\frac{3}{2})_2$	$1272800+x$	1273588	1274670	1273846	1272663	1.806[−03]	2.236[−03]	2.272[−03]	2.78[−03]
$^3F^o_4$	$(\frac{3}{2},\frac{5}{2})_4$	$1389120+x$	1393177	1395047	1392887	1386631	4.244[−05]	4.040[−05]	4.071[−05]	4.08[−05]
$^1D^o_2$	$(\frac{3}{2},\frac{5}{2})_2$	[1409000]	1408207	1409714	1408445	1407083	1.669[−05]	1.681[−05]	1.688[−05]	2.20[−05]
$^3D^o_3$	$(\frac{3}{2},\frac{5}{2})_3$	$1451660+x$	1452487	1453759	1452685	1452370	1.614[−05]	1.634[−05]	1.642[−05]	1.64[−05]
$^3D^o_1$	$(\frac{3}{2},\frac{5}{2})_1$	1565350	1566184	1561730	1571375	1579125	1.383[−12]	1.592[−12]	1.636[−12]	1.59[−12]
$^3F^o_2$	$(\frac{1}{2},\frac{3}{2})_2$		1987261	1986787	1985683	1985853	1.396[−07]	1.426[−07]	1.419[−07]	1.43[−07]
$^1P^o_1$	$(\frac{1}{2},\frac{3}{2})_1$	2142690	2145671	2138019	2152772	2167239	3.603[−13]	4.443[−13]	4.823[−13]	4.45[−13]
$^3P^o_2$	$(\frac{1}{2},\frac{5}{2})_2$		2146087	2146119	2144754		1.407[−07]	1.434[−07]	1.426[−07]	1.44[−07]
$^1F^o_3$	$(\frac{1}{2},\frac{5}{2})_3$		2168024	2167712	2166530	2168010	1.274[−07]	1.308[−07]	1.302[−07]	1.31[−07]

Table 2: Convergence of excitation energies (in cm^{-1}) for levels belonging to the even $4p^6$ and odd parity $4p^5 4d$ configurations of W^{38+} from the present MCDHF calculations, for each of the three applied correlation models. The first column gives an the LSJ term, also including parity to distinguish between the even and odd states. The second column gives Dirac-Hartree-Fock (DHF) values for the Dirac-Coulomb (DC) operator and the following four columns show how the total excitation energies change with inclusion of more and more electron correlation according to the VV, CV_{3d} and CV_{3p} active set (AS) models defined in the theory section. Column seven to nine give the contribution from Breit, Self-Energy (SE) and Vacuum Polarization (VP) and the last column shows the total excitation energies including these effects. The CV_{3p} model present the most accurate values.

Term	DHF	VV							
	DC	DC				BQ			DC+BQ
		AS_1	AS_2	AS_3	AS_4	Breit	SE	VP	AS_4
$^1S^e_0$	0	0	0	0	0	0	0	0	0
$^3P^o_0$	1203050	1210284	1210478	1209211	1209050	-3651	-1464	5	1203940
$^3P^o_1$	1240964	1247364	1247156	1245712	1245542	-4306	-1447	5	1239794
$^3F^o_3$	1267763	1273740	1272950	1271205	1271021	-4493	-1460	6	1265072
$^3D^o_2$	1277681	1282175	1281657	1279939	1279753	-4134	-1462	7	1274162
$^3F^o_4$	1397505	1405036	1404908	1403040	1402878	-7881	-1215	3	1393784
$^1D^o_2$	1415083	1419394	1419533	1417617	1417450	-7478	-1224	6	1408752
$^3D^o_3$	1460445	1464801	1464343	1462102	1461916	-7462	-1223	5	1453234
$^3D^o_1$	1589796	1584046	1583267	1580706	1580525	-7461	-1220	18	1571860
$^3F^o_2$	2000563	2001067	2000733	1999034	1998859	-11900	-922	228	1986259
$^3P^o_2$	2162636	2162421	2162626	2160662	2160494	-14712	-689	227	2145316
$^1P^o_1$	2183616	2169764	2168500	2165845	2165652	-11492	-948	213	2153420
$^1F^o_3$	2185105	2185452	2185212	2183022	2182848	-15204	-685	228	2167180

Term	DHF	CV_{3d}							
	DC	DC				BQ			DC+BQ
		AS_1	AS_2	AS_3	AS_4	Breit	SE	VP	AS_4
$^1S^e_0$	0	0	0	0	0	0	0	0	0
$^3P^o_0$	1203050	1211736	1211876	1210277	1209486	-3718	-1462	5	1204310
$^3P^o_1$	1240964	1248836	1248442	1246618	1245785	-4388	-1446	5	1239956
$^3F^o_3$	1267763	1275321	1274347	1272151	1271274	-4594	-1460	5	1265225
$^3D^o_2$	1277681	1283794	1282993	1280763	1279880	-4231	-1461	5	1274193
$^3F^o_4$	1397505	1406573	1405690	1403846	1403018	-8024	-1214	3	1393782
$^1D^o_2$	1415083	1420963	1420330	1418412	1417561	-7617	-1223	5	1408725
$^3D^o_3$	1460445	1466380	1465078	1462805	1461894	-7613	-1222	4	1453062
$^3D^o_1$	1589796	1582841	1579598	1577122	1576113	-7592	-1220	16	1567316
$^3F^o_2$	2000563	2002930	2003218	2001078	2000241	-11890	-920	227	1987655
$^3P^o_2$	2162636	2164234	2163139	2160277	2159216	-14743	-685	227	2146536
$^1P^o_1$	2183616	2167079	2164531	2162575	2161742	-11543	-942	214	2146940
$^1F^o_3$	2185105	2187254	2187100	2184960	2184107	-15251	-682	227	2168397

Term	DHF	CV_{3p}							
	DC	DC				BQ			DC+BQ
		AS_1	AS_2	AS_3	AS_4	Breit	SE	VP	AS_4
$^1S^e_0$	0	0	0	0	0	0	0	0	0
$^3P^o_0$	1203050	1211718	1210623	1209201	1208694	-3666	-1463	5	1203570
$^3P^o_1$	1240964	1248761	1247314	1245766	1245213	-4345	-1446	5	1239427
$^3F^o_3$	1267763	1275240	1273130	1271431	1270820	-4583	-1460	5	1264782
$^3D^o_2$	1277681	1283606	1281635	1279861	1279248	-4206	-1461	7	1273588
$^3F^o_4$	1397505	1406567	1404446	1402955	1402386	-7997	-1215	3	1393177
$^1D^o_2$	1415083	1420902	1419147	1417596	1417013	-7587	-1224	5	1408207
$^3D^o_3$	1460445	1466268	1463731	1461977	1461318	-7613	-1222	4	1452487
$^3D^o_1$	1589796	1582542	1577719	1575901	1575061	-7673	-1220	16	1566184
$^3F^o_2$	2000563	2002892	2002185	2000525	1999893	-11939	-920	227	1987261
$^1P^o_1$	2183616	2166644	2161107	2159088	2158129	-11729	-942	213	2145671
$^3P^o_2$	2162636	2164236	2163521	2161965	2161339	-14794	-685	227	2146087
$^1F^o_3$	2185105	2187301	2186067	2184459	2183805	-15325	-683	227	2168024

Table 3: MCDHF-CV$_{3p}$ transition data for all of the transitions of E1, M1, E2, M2, E3 from $4p^6$ and $4p^5 4d$ configuration, the transition wavelength λ (in nm), transition rate A^r (in s^{-1}, length form), oscillator strength gf (in a.u., length form), and line strength S (in a.u., length form). The accuracy indicator δS for line strength and the branching ratio of transition rate B_F (in %) are also listed. $a[\pm b] = a \times 10^{\pm b}$.

Transition	λ	EM	A^r	gf	S	δS	B_F
$^3P_1^o - {}^1S_0^e$	8.0683	$E1$	2.633[+09]	7.710[−03]	2.048[−03]	0.046	100
$^3P_1^o - {}^3P_0^o$	278.886	$M1$	6.108[+02]	2.137[−06]	1.474[+00]		0
$^3F_3^o - {}^1S_0^e$	7.9065	$E3$	2.108[+01]	1.383[−10]	9.065[−03]	0.000	100
$^3D_2^o - {}^1S_0^e$	7.8518	$M2$	8.835[+01]	4.083[−10]	8.843[−02]		20
$^3D_2^o - {}^3P_1^o$	292.731	$M1$	3.455[+02]	2.220[−06]	1.607[+00]		79
$^3D_2^o - {}^3F_3^o$	135.689	$M1$	6.254[+00]	6.047[−07]	1.698[+00]		1
$^3F_4^o - {}^3F_3^o$	77.8848	$M1$	2.455[+04]	2.010[−05]	3.871[+00]		100
$^3F_4^o - {}^3D_2^o$	83.6193	$E2$	1.008[+00]	9.508[−10]	3.311[−03]	0.090	0
$^1D_2^o - {}^1S_0^e$	7.1012	$M2$	1.392[+04]	5.261[−08]	8.428[+00]		24
$^1D_2^o - {}^3P_0^o$	48.8669	$E2$	2.498[+01]	4.471[−09]	3.107[−03]	0.044	0
$^1D_2^o - {}^3P_1^o$	59.2485	$M1$	3.115[+04]	8.196[−06]	1.201[+00]		53
$^1D_2^o - {}^3F_3^o$	69.7229	$M1$	2.063[+03]	7.517[−07]	1.296[−01]		4
$^1D_2^o - {}^3D_2^o$	74.2834	$M1$	1.209[+04]	5.003[−06]	9.190[−01]		20
$^3D_3^o - {}^1S_0^e$	6.8847	$E3$	5.092[+01]	2.533[−10]	8.311[−03]	0.000	0
$^3D_3^o - {}^3P_1^o$	46.9351	$E2$	1.694[+01]	3.916[−09]	2.412[−03]	0.053	0
$^3D_3^o - {}^3F_3^o$	53.2752	$M1$	1.550[+04]	4.617[−06]	6.082[−01]		25
$^3D_3^o - {}^3D_2^o$	55.8974	$M1$	4.522[+04]	1.483[−05]	2.050[+00]		74
$^3D_3^o - {}^3F_4^o$	168.607	$M1$	7.068[+01]	2.109[−07]	8.791[−02]		0
$^3D_3^o - {}^1D_2^o$	225.837	$M1$	2.406[+01]	1.288[−07]	7.191[−02]		0
$^3D_1^o - {}^1S_0^e$	6.3850	$E1$	6.112[+11]	1.121[+00]	2.356[−01]	0.026	100
$^3D_1^o - {}^3P_0^o$	27.5775	$M1$	1.511[+05]	5.169[−06]	3.525[−01]		0
$^3D_1^o - {}^3P_1^o$	30.6037	$M1$	2.186[+05]	9.210[−06]	6.970[−01]		0
$^3D_1^o - {}^3F_3^o$	33.1783	$E2$	3.568[+02]	1.766[−08]	3.842[−03]	0.059	0
$^3D_1^o - {}^3D_2^o$	34.1768	$M1$	1.235[+05]	6.487[−06]	5.482[−01]		0
$^3D_1^o - {}^1D_2^o$	63.3004	$M1$	1.179[+03]	2.125[−07]	3.327[−02]		0
$^3D_1^o - {}^3D_3^o$	87.9528	$E2$	4.746[+00]	1.651[−09]	6.692[−03]	0.164	0
$^3F_2^o - {}^1S_0^e$	5.0321	$M2$	1.787[+03]	3.391[−09]	1.933[−01]		0
$^3F_2^o - {}^3P_0^o$	12.7601	$E2$	4.299[+04]	5.247[−07]	6.492[−03]	0.015	1
$^3F_2^o - {}^3P_1^o$	13.3720	$M1$	3.228[+05]	4.326[−06]	1.431[−01]		5
$^3F_2^o - {}^3F_3^o$	13.8412	$M1$	4.736[+06]	6.801[−05]	2.328[+00]		67
$^3F_2^o - {}^3D_2^o$	14.0120	$M1$	1.662[+06]	2.446[−05]	8.477[−01]		24
$^3F_2^o - {}^3F_4^o$	16.8327	$E2$	1.734[+01]	3.682[−10]	1.046[−05]	0.151	0
$^3F_2^o - {}^1D_2^o$	17.2696	$M1$	1.236[+04]	2.763[−07]	1.180[−02]		0
$^3F_2^o - {}^3D_3^o$	18.6995	$M1$	7.000[+03]	1.835[−07]	8.484[−03]		0
$^3F_2^o - {}^3D_1^o$	23.7487	$M1$	1.174[+04]	4.964[−07]	2.915[−02]		0
$^1P_1^o - {}^1S_0^e$	4.6606	$E1$	2.073[+12]	2.025[+00]	3.108[−01]	0.012	100
$^1P_1^o - {}^3P_0^o$	10.6146	$M1$	1.215[+06]	6.158[−06]	1.616[−01]		0
$^1P_1^o - {}^3P_1^o$	11.0346	$M1$	2.886[+06]	1.580[−05]	4.313[−01]		0
$^1P_1^o - {}^3F_3^o$	11.3522	$E2$	4.612[+05]	2.673[−06]	2.329[−02]	0.017	0
$^1P_1^o - {}^3D_2^o$	11.4668	$M1$	3.179[+06]	1.880[−05]	5.330[−01]		0
$^1P_1^o - {}^1D_2^o$	13.5600	$M1$	1.489[+04]	1.232[−07]	4.130[−03]		0
$^1P_1^o - {}^3D_3^o$	14.4262	$E2$	3.785[+03]	3.543[−08]	6.335[−04]	0.078	0
$^1P_1^o - {}^3D_1^o$	17.2566	$M1$	1.587[+05]	2.126[−06]	9.071[−02]		0
$^1P_1^o - {}^3F_2^o$	63.1272	$M1$	1.168[+03]	2.093[−07]	3.267[−02]		0
$^3P_2^o - {}^1S_0^e$	4.6596	$M2$	1.522[+04]	2.476[−08]	1.121[+00]		0
$^3P_2^o - {}^3P_0^o$	10.6099	$E2$	5.780[+02]	4.878[−09]	3.470[−05]	0.118	0
$^3P_2^o - {}^3P_1^o$	11.0295	$M1$	1.678[+05]	1.530[−06]	4.173[−02]		2
$^3P_2^o - {}^3F_3^o$	11.3468	$M1$	5.154[+03]	4.974[−08]	1.396[−03]		0
$^3P_2^o - {}^3D_2^o$	11.4613	$M1$	1.892[+04]	1.863[−07]	5.280[−03]		0
$^3P_2^o - {}^3F_4^o$	13.2818	$E2$	2.080[+05]	2.751[−06]	3.838[−02]	0.002	3
$^3P_2^o - {}^1D_2^o$	13.5523	$M1$	2.763[+06]	3.804[−05]	1.275[+00]		39
$^3P_2^o - {}^3D_3^o$	14.4175	$M1$	2.025[+06]	3.155[−05]	1.125[+00]		29
$^3P_2^o - {}^3D_1^o$	17.2443	$M1$	1.690[+06]	3.767[−05]	1.606[+00]		24

Table 3: (*continued*)

Transition	λ	EM	A^r	gf	S	δS	B_F
$^3P^o_2 - {}^3F^o_2$	62.9617	$M1$	3.336[+03]	9.914[−07]	1.544[−01]		0
$^1F^o_3 - {}^1S^e_0$	4.6125	$E3$	8.608[+02]	1.922[−09]	8.512[−03]	0.003	0
$^1F^o_3 - {}^3P^o_1$	10.7689	$E2$	1.721[+04]	2.094[−07]	1.558[−03]	0.037	0
$^1F^o_3 - {}^3F^o_3$	11.0712	$M1$	5.634[+03]	7.248[−08]	1.984[−03]		0
$^1F^o_3 - {}^3D^o_2$	11.1802	$M1$	3.594[+03]	4.715[−08]	1.303[−03]		0
$^1F^o_3 - {}^3F^o_4$	12.9058	$M1$	4.837[+06]	8.454[−05]	2.698[+00]		63
$^1F^o_3 - {}^1D^o_2$	13.1611	$M1$	5.954[+05]	1.082[−05]	3.523[−01]		8
$^1F^o_3 - {}^3D^o_3$	13.9755	M1	1.878[+06]	3.850[−05]	1.330[+00]		24
$^1F^o_3 - {}^3D^o_1$	16.6157	E2	2.134[+04]	6.181[−07]	1.689[−02]	0.019	0
$^1F^o_3 - {}^3F^o_2$	55.3210	M1	5.806[+04]	1.865[−05]	2.551[+00]		1
$^1F^o_3 - {}^3P^o_2$	455.860	M1	3.673[+01]	8.011[−07]	9.031[−01]		0

Table 4: Comparison of computed wavelengths from different theories with experimental wavelengths for observable lines ($B_F > 20\%$). *a* - [23]; *b* - [21]; *c* - Present theoretical work; *d* - [25]; *e* - [24], *f* - [23].

Transition	EM	$\lambda^a_{\rm Exp}$	$\lambda^c_{\rm CV_{3p}}$	$\lambda^c_{\rm RMBPT}$	$\lambda^d_{\rm MCDHF}$	$\lambda^e_{\rm RELAC}$	$\lambda^f_{\rm HULLAC}$
$^3P^o_1-{}^1S^e_0$	E1	8.064	8.068	8.058	8.068	8.0886	8.0897
$^3F^o_3-{}^1S^e_0$	E3		7.907	7.901			
$^3D^o_2-{}^1S^e_0$	M2		7.852	7.845			
$^3D^o_2-{}^3P^o_1$	M1		292.73	296.59	290.715		275.88
$^3F^o_4-{}^3F^o_3$	M1	79.923	77.885	77.324	77.946		79.8080
$^1D^o_2-{}^1S^e_0$	M2		7.101	7.094			
$^1D^o_2-{}^3P^o_1$	M1		59.249	59.256	59.172		58.5986
$^1D^o_2-{}^3D^o_2$	M1		74.283	74.050			
$^3D^o_3-{}^3F^o_3$	M1	53.287	53.275	53.181	53.166		52.367
$^3D^o_3-{}^3D^o_2$	M1	55.904	55.897	55.838			55.6759
$^3D^o_1-{}^1S^e_0$	E1	6.3883 6.398[b]	6.385	6.403	6.364	6.3326	6.3249
$^3F^o_2-{}^3F^o_3$	M1		13.841	13.868	13.868	13.1804	13.809
$^3F^o_2-{}^3D^o_2$	M1		14.012	14.043			
$^1P^o_1-{}^1S^e_0$	E1	4.667 4.640[b]	4.661	4.677	4.645	4.6142	4.6064
$^3P^o_2-{}^1D^o_2$	M1		13.552	13.580			
$^3P^o_2-{}^3D^o_3$	M1		14.418	14.443			
$^3P^o_2-{}^3D^o_1$	M1		17.244	17.112			
$^1F^o_3-{}^3F^o_4$	M1		12.906	12.942	12.926	12.7979	12.805
$^1F^o_3-{}^3D^o_3$	M1		13.976	14.007			